IEEE Access
Multidisciplinary | Rapid Review | Open Access Journal

Received November 19, 2020, accepted December 16, 2020, date of publication December 23, 2020,
date of current version January 11, 2021.

*Digital Object Identifier 10.1109/ACCESS.2020.3046728*

# Practical Real-Time Implementation of a Disturbance Rejection Control Scheme for a Twin-Rotor Helicopter System Using Intelligent Active Force Control

**SHERIF I. ABDELMAKSOUD[1], MUSA MAILAH[1], (Senior Member, IEEE), AND AYMAN M. ABDALLAH[2]**

[1]School of Mechanical Engineering, Universiti Teknologi Malaysia (UTM), Johor Bahru 81310, Malaysia
[2]Aerospace Engineering Department, King Fahd University of Petroleum and Minerals, Dhahran 31261, Saudi Arabia

Corresponding author: Sherif I. Abdelmaksoud (iasherif@graduate.utm.my)

**ABSTRACT** This paper centers around an experimental investigation into the effectiveness of an innovative hybrid control approach based on an intelligent active force control (IAFC) strategy to stabilize a twin-rotor helicopter model and improve its ability to reject external disturbances efficiently. The intelligent algorithm was based on an iterative learning (IL) method integrated into the main control loop to estimate control parameters automatically while on-line. A mechatronic test rig with the IAFC-based control algorithm was incorporated into a *Quanser Aero* twin-rotor model in a laboratory setting as a verification platform to evaluate the applicability and efficacy of the proposed control algorithm via a practical real-time implementation. The hybrid IAFC-based control design was rigorously examined to test its feasibility and durability in countering various forms of external disturbances while executing the trajectory tracking tasks. Notably, the efficiency of the IAFC-based control unit was mainly studied and compared with other control plans under different operating conditions for benchmarking. The experimental results show the ability of the controller based on the IAFC strategy to effectively improve the disturbance rejection capability compared to the other control schemes considered in the study. About 27% improvement of the system performance in terms of lowering the root mean square error (RMSE) was observed compared to the other control systems counterparts.

**INDEX TERMS** Twin-rotor system, 2-DOF helicopter model, rotorcraft UAVs, active force control, intelligent system, iterative learning, experimental test rig, disturbance rejection.

## I. INTRODUCTION

Unmanned aerial vehicle (UAV) is a broad topic of interest much discussed in recent years. The subject matter receives much attention due to the fact that UAVs have many desirable features, including small size and weight, high-mobility, and self-stabilizing, allowing them to be used in a wide range of applications such as search and rescue (SAR) mission, remote sensing, real-time monitoring, and meteorological reconnaissance. Among the different types of UAVs, a twin-rotor helicopter is considered one of the most versatile and vital modes of transportation nowadays. Unlike fixed-wing aircraft, it can vertically take off and land (VTOL) without a runway, hover in one spot, perform quick maneuvering, and fly backward or sideways. Besides, it is also utilized in a wide range of applications with particular reference to the military and civilian sectors. However, it is known to be multi-variable, highly non-linear, and strongly coupled system [1]. It also faces several impediments during tracking specific paths such as instability, moving and fixed obstacles, motors failure, external disturbances, and model uncertainties. Hence, the existence of a robust and effective control system is deemed necessary.

A two-degree of freedom (2-DOF) helicopter is an example of a UAV commonly used as a dual-rotor laboratory experimental rig to practically test the effectiveness of proposed

The associate editor coordinating the review of this manuscript and approving it for publication was Fei Chen.

control strategies that may be applied and implemented to a real helicopter system.

Several research works have been conducted to develop the control techniques for the 2-DOF helicopter over the past decades to provide robust solutions in demanding environments. Amongst the various impediments encountered by the helicopter system are ensuring stabilized motion maneuvering during trajectory tracking and rejecting various forms of external disturbances. Pandey *et al*. [2] implemented both in simulation and experimentation a robust proportional–integral–derivative (PID) controller tuned using a bacterial foraging optimization (BFO) method, to solve the stabilizing problem of a twin-rotor helicopter subjected to actuator nonlinearity, disturbances, and uncertainties, on the basis of *Kharitonov* robust stability criteria. However, the PID compensation is not able to reject various types of disturbances or model uncertainties, and that its performance is strongly influenced by the coupling effect as well. With regard to conventional PID controllers in different operating conditions, they are unable to deliver the desired performance under various forms of disturbances [3]. Thus, Ijaz *et al*. [4] proposed a fractional order PID (FOPID) controller adjusted using the *Nelder Mead* (NM) optimization method and compared its effectiveness with both a FOPID controller tuned using the PSO technique and traditional PID. The results showed better effectiveness and less control effort of the NM-based FOPID method compared with other control schemes, in the presence of disturbances. Moreover, Ali *et al.* [5] designed a disturbance observer through $H_\infty$-based approach for solving the problem of disturbance rejection for a twin-rotor aerodynamic system. A robust fault estimation method using $H_\infty$ approach to achieve certain disturbance level attenuation with observer convergence in the presence of external disturbances and unknown input was presented in [6].

With respect to non-linear controllers, Rojas-Cubides *et al.* [7] suggested a robust control scheme combining a first-order sliding mode control (SMC) approach with a high-order generalized proportional integral (GPI) observer to handle fault and parametric uncertainties, non-linearities, and external disturbances. They verified the simulation results experimentally on a 2-DOF helicopter system. Faris *et al*. [8] also demonstrated a real-time implementation of a decentralized SMC for a twin-rotor MIMO system (TRMS) that revealed the efficacy and robustness of the proposed controller in stabilizing and efficiently rejecting the external disturbances. Moreover, Rashad *et al*. [9] investigated, experimentally and analytically, a robust tracking controller for a helicopter system subjected to external disturbances and model uncertainties with a partial failure in the actuator, by utilizing integral sliding mode disturbances observer sliding mode control (SMDO-SMC). The results exhibited that the suggested control approach could provide less tracking error with lower control action and effective behavior due to the parametric uncertainty.

Additionally, Ilyas *et al*. [10] designed a first-order SMC and backstepping controller (BC) schemes for dealing with the oscillations and chattering effects in the pitch and yaw angles in the presence of parametric uncertainties and external disturbances. The results showed better effectiveness of the BC in giving efficient behavior and reducing the oscillations and chattering compared to the SMC. Raghavan and Thomas [11] implemented a practical model predictive control (MPC) for solving the coupling and non-linearities consequences to achieve efficient tracking performance. The results presented that the proposed strategy is effective and robust in tracking desired trajectories without violating the control input constraints and rejecting the external disturbances and coupling impacts. Furthermore, Zeghlache and Amardjia [12] applied a fuzzy SMC based on the non-linear observer experimentally to control and stabilize a twin-rotor helicopter against coupling, non-linearities, uncertainties, and external disturbances to achieve accurate tracking.

One promising strategy is to utilize an active disturbance rejection control (ADRC) approach to achieve the desired motions with the ability to fend off disturbances. Najm and Ibraheem [13] presented an improved ADRC technique consisting of an improved tracking differentiator, a linear extended state observer, and a non-linear PID controller to stabilize a rotorcraft model and efficiently expel the exogenous disturbances and uncertainties. Yang *et al*. [14] also presented, a practical composite control strategy based on ADRC and feed-forward input shaping technique. Both the analytical and experimental results demonstrated the viability and robustness of the suggested approach compared to a conventional PID controller in rejecting the external disturbances and sudden parametric changes. However, the control structure is complex, and many control parameters need to be tuned.

Another emerging robust control strategy is called active force control (AFC) that was first demonstrated by Hewit and Burdess in the early eighties based on the classical *Newton's* second law of motion [15]. It has the ability to expel any known/ unknown or external/internal disturbances in normal or complex environments while ensuring system stability. It can be readily combined with the classical, modern, or intelligent control systems. In work done in [3], intelligent active force control (IAFC)-based controller has been implemented to fend off the external disturbances for a single link robot arm. Meanwhile, Tahmasebi *et al.* [16] applied the active torque control with iterative learning to suppress the vibrational levels of a sprayer boom structure. Sharif and Mailah [17] developed a practical and robust control method that combined the PID controller with the AFC strategy to regulate a feed flow rate of a syringe fluid dispensing system by controlling the speed of a DC motor. Based on previous studies, the results revealed the ability of the AFC strategy in improving the system performance and rejecting the external disturbances.

Regarding rotorcraft UAVs [18], some research works have been reported in [19] and [20], which combined the AFC strategy analytically with a PID controller to stabilize the 2-DOF helicopter model and compensate for the disturbances. The simulated results showed the effectiveness and robustness of the AFC-based technique. A research work is also reported in [21] that utilized an AFC-based control scheme to control a quadrotor model. The proposed control system combined a PID controller with the AFC, which was tuned by a trial-and-error method (TEM) for controlling only the altitude and yaw motions. The results showed that the PID-AFC strategy significantly improved the altitude control with a much faster response than a conventional PID controller. Additionally, Abdelmaksoud *et al*. [22] presented an innovative hybrid control scheme for a multi-rotor model to improve the disturbances rejection capability by utilizing an AFC-based robust intelligent control system via a simulation study. However, there is as yet no research work has been carried out in relation to the practical implementation of the IAFC strategy on the UAV systems to assess its viability in enhancing the disturbance rejection capability and its agreement with the simulation results counterpart.

The main objective of this study is to evaluate the performance of a practical and real-time implementation of the IAFC-based controller in improving the disturbance rejection capability of a twin-rotor helicopter model in the presence of external disturbances in a laboratory environment. The focus is more on demonstrating the novelty of this research through the development of an experimental test rig based on a selected rotorcraft system to imply the effectiveness, simplicity, and durability of incorporating the IAFC-based control strategy into the UAV system, as well as its ability to be seamlessly integrated with intelligent control elements for real-time application.

The remainder of this paper is organized as follows: Section 2 describes the mathematical model of a 2-DOF helicopter system under specific assumptions. Then, the designed PID controller and proposed IAFC technique with iterative learning are presented in Section 3. Section 4 presents the experimental setup, while Section 5 shows the experimental results and performance analysis for the trajectory tracking tests based on the prescribed operating and loading conditions. Finally, the paper's conclusion is given in Section 6.

## II. MODELING THE SYSTEM DYNAMICS

In the following sections, the mathematical model of a 2-DOF helicopter system was derived based on the *Euler-Lagrange* approach considering the coupling effects and various types of disturbances.

### A. 2-DOF HELICOPTER SYSTEM MODELING

The mathematical model of the 2-DOF helicopter model was derived according to work done in [23]. The 2-DOF helicopter platform is shown in **Figure 1,** where it was derived based on the following assumptions [1]:

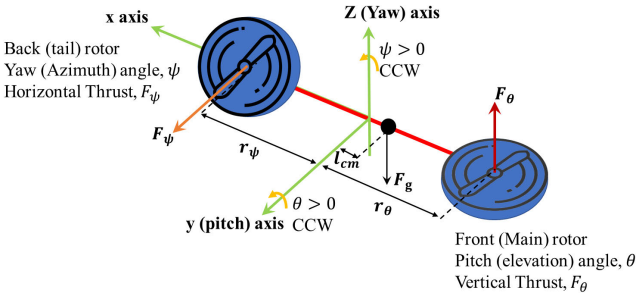


**FIGURE 1.** The free-body diagram of the 2-DOF helicopter model.

1. The main and back rotors are of the same size and equidistant from each other.
2. Both the front and back rotors generate a torque on each other.
3. The model is horizontal and parallel with the ground when the pitch angle is zero.
4. The pitch angle increases positively when the front rotor is moved upwards, the body rotates CCW about the $y$-axis, and the front rotor voltage is positive.
5. The yaw angle increases positively when the body rotates CCW about the $z$-axis, and the back-rotor voltage is positive.
6. As the system is fixed, it cannot rotate around the roll axis or move along the axis.

It is necessary to study the behavior of the center of mass to derive the model of the 2-DOF helicopter. It is worth mentioning that the center of mass displaces a distance, $l_{\rm cm}$ on the $x$-axis, as shown in **Figure 1**. Thus, the center of mass after the transformation of the coordinates, utilizing the pitch and yaw rotation matrices, is as follows:

$$\begin{aligned} X_{\rm cm} &= l_{\rm cm}\cos\psi\cos\theta \\ Y_{\rm cm} &= l_{\rm cm}\sin\psi\cos\theta \\ Z_{\rm cm} &= l_{\rm cm}\sin\theta \end{aligned} \tag{1}$$

Where

$\theta$ and $\psi$ : pitch and yaw angles, respectively
$l_{\rm cm}$ : distance of the center of mass and the intersection of the pitch and yaw axes

The center of mass is represented by the *Cartesian* coordinates with respect to the pitch and yaw angles. Based on the *Euler-Lagrange* formulation and the free body diagram of the 2-DOF helicopter in **Figure 1**, the total potential energy ($PE$) of the system due to gravity is:

$$PE = m_{\rm h} g l_{\rm cm}\sin\theta \tag{2}$$

The total kinetic energy ($KE$), with reference to **Figure 1,** is the combination of the rotational kinetic energies acting on the pitch and yaw axes, respectively, along with the translational kinetic energy generated by the movement of the center

of mass and is given by:

$$\begin{aligned} KE &= \frac{1}{2}J_\theta\dot{\theta}^2 + \frac{1}{2}J_\psi\dot{\psi}^2 \\ &+\frac{1}{2}m_{\mathrm{h}}\Big[\left(-\sin(\psi)\,\dot{\psi}\cos(\theta)\,l_{\mathrm{cm}} - \cos(\psi)\sin(\theta)\,\dot{\theta}l_{\mathrm{cm}}\right)^2 \\ &+\left(-\cos(\psi)\,\dot{\psi}\cos(\theta)\,l_{\mathrm{cm}} + \sin(\psi)\sin(\theta)\,\dot{\theta}l_{\mathrm{cm}}\right)^2 \\ &+\cos(\theta)^2\dot{\theta}^2 l_{\mathrm{cm}}^2\Big] \end{aligned} \tag{3}$$

where

$J_\theta, J_\psi$ : total moment of inertia about the pitch and yaw axes, respectively
$m_{\mathrm{h}}$ : total moving mass
g : acceleration due to gravity

The torques generated at the pitch and yaw axes are a function of the voltages applied to the motors, such as:

$$\begin{aligned} \tau_\theta(t) &= K_{\theta\theta}u_\theta(t) + K_{\theta\psi}u_\psi(t) \\ \tau_\psi(t) &= K_{\psi\theta}u_\theta(t) + K_{\psi\psi}u_\psi(t) \end{aligned} \tag{4}$$

where

$\tau_\theta(t), \tau_\psi(t)$ : control torques act on the pitch axis and yaw axis, respectively
$u_\theta(t), u_\psi(t)$ : control actions applied as motor voltages to the pitch and yaw rotors, respectively
$K_{\theta\theta}$ : torque thrust gain from the pitch rotor
$K_{\theta\psi}$ : cross-torque thrust gain acting on the pitch from the yaw rotor
$K_{\psi\theta}$ : cross-torque thrust gain acting on the yaw from the pitch rotor
$K_{\psi\psi}$ : torque thrust gain from the yaw rotor

The generalized forces vector is given by:

$$\begin{aligned} Q = [Q_1, Q_2] = \big[&K_{\theta\theta}u_\theta(t) + K_{\theta\psi}u_\psi(t) \\ &-D_\theta\dot{\theta}(t), K_{\psi\theta}u_\theta(t) + K_{\psi\psi}u_\psi(t) - D_\psi\dot{\psi}(t)\big] \end{aligned} \tag{5}$$

where $D_\theta$ and $D_\psi$ are damping coefficients about the pitch and yaw axes, respectively. From the *Lagrangian* of the system, the non-conservative forces of the system are written as:

$$\begin{aligned} L &= KE - PE \\ \frac{\partial}{\partial t}\frac{\partial L}{\partial \dot{q}_1} - \frac{\partial}{\partial q_1}L &= Q_1 \\ \frac{\partial}{\partial t}\frac{\partial L}{\partial \dot{q}_2} - \frac{\partial}{\partial q_2}L &= Q_2 \end{aligned} \tag{6}$$

where

$q_1$ & $q_2$ : generalized coordinates related to $\theta$ and $\psi$, respectively
$L$ : *Lagrangian* function - the difference between the total kinetic and potential energies of the system

Based on the *Euler-Lagrange* formulation, the non-linear dynamic equation that describes the pitch and yaw attitude motions relative to the motor are given as [1]:

$$\left(J_\theta + m_{\mathrm{h}}l_{\mathrm{cm}}^2\right)\ddot{\theta} + D_\theta\dot{\theta} + \alpha + \beta = K_{\theta\theta}u_\theta + K_{\theta\psi}u_\psi \tag{7}$$

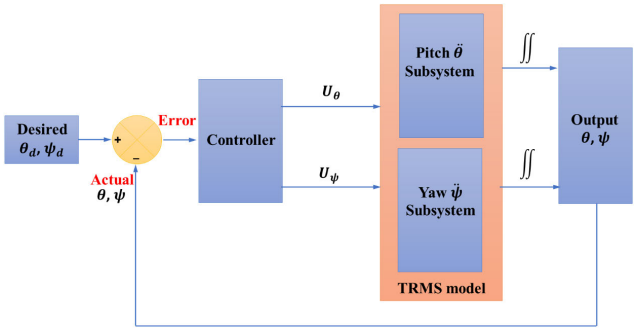


**FIGURE 2.** The schematic block diagram of a 2-DOF helicopter model.

where

$$\begin{aligned} \alpha &= m_{\mathrm{h}}l_{\mathrm{cm}}^2\dot{\psi}^2\sin(\theta)\cos(\theta) \\ \beta &= m_{\mathrm{h}}gl_{\mathrm{cm}}\cos(\theta) \end{aligned}$$

$$\left(J_\psi + m_{\mathrm{h}}l_{\mathrm{cm}}^2\cos(\theta)^2\right)\ddot{\psi} + D_\psi\dot{\psi} - \gamma = K_{\psi\theta}u_\theta + K_{\psi\psi}u_\psi \tag{8}$$

where

$$\gamma = 2m_{\mathrm{h}}l_{\mathrm{cm}}^2\sin(\theta)\cos(\theta)\,\dot{\theta}\dot{\psi}$$

Defining the state vector of the 2-DOF helicopter model as follows:

$$X = [x_1\ x_2\ x_3\ x_4] \tag{9}$$

where it represents the DOF as follows:

$$X = [\theta\ \psi\ \dot{\theta}\ \dot{\psi}] \tag{10}$$

The state-space representation is expressed as:

$$\begin{aligned} [\dot{X}] &= \begin{bmatrix} x_3 \\ x_4 \\ \frac{K_{\theta\theta}u_\theta + K_{\theta\psi}u_\psi - D_\theta x_3 - m_{\mathrm{h}}l_{\mathrm{cm}}^2x_4^2\sin(x_1)\cos(x_1) - m_{\mathrm{h}}gl_{\mathrm{cm}}\cos(x_1)}{(J_\theta + m_{\mathrm{h}}l_{\mathrm{cm}}^2)} \\ \frac{K_{\psi\theta}u_\theta + K_{\psi\psi}u_\psi - D_\psi x_4 + 2m_{\mathrm{h}}l_{\mathrm{cm}}^2\sin(x_1)\cos(x_1)x_3x_4}{(J_\psi + m_{\mathrm{h}}l_{\mathrm{cm}}^2\cos(x_1)^2)} \end{bmatrix} \end{aligned} \tag{11}$$

The schematic block diagram of a 2-DOF helicopter model is shown in **Figure 2**.

## III. CONTROL SYSTEM DESIGN

In this section, after deriving the mathematical model of the 2-DOF helicopter system, the proposed IAFC based control scheme, which is the AFC with the iterative learning (PID-AFC-IL), was designed, developed, and subsequently compared with the PID and PID-AFC control systems to analyze their effectiveness during trajectory tracking, as described in the following sections.

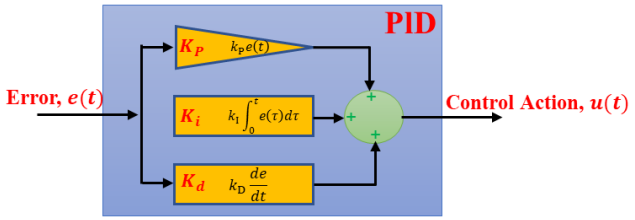


**FIGURE 3.** Schematic diagram of a PID controller.

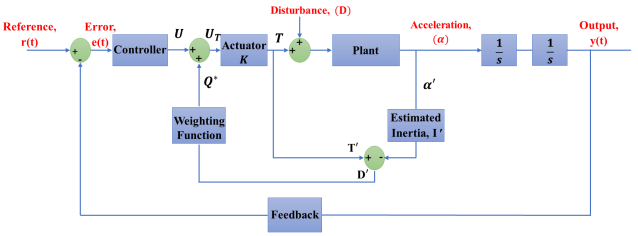


**FIGURE 4.** Schematic diagram of the AFC technique.

### A. PROPORTIONAL–INTEGRAL–DERIVATIVE (PID)

A PID controller is a relatively robust linear controller that is very popular in the industry and can be employed in a wide range of linear and non-linear applications due to its simplicity and reliability. The PID principally consists of three gains (controller parameters); the proportional term ($K_P$) that describes the current error, the integral term ($K_I$) which expresses the accumulated past error and the derivative term ($K_D$) that predicts the future error for providing the best control signal. The schematic diagram of the PID control system is shown in **Figure 3**.

To design a PID controller, generally, the following equation is utilized:

$$G(s) = K_P + \frac{K_I}{s} + K_D s \tag{12}$$

Therefore, the output signal of the PID controller can be expressed as:

$$m(s) = G(s)\, e(s) = K_P e(s) + \frac{K_I e(s)}{s} + K_D s e(s) \tag{13}$$

where $e(s)$ is the error and defined as:

$$e(s) = \text{Reference} - \text{Output} \tag{14}$$

Based on the mathematical model of the 2-DOF helicopter, a PID controller was designed for the yaw angle. In contrast, another PID control system with a feed-forward term was considered to regulate the pitch angle. The non-linear feed-forward term for the pitch angle compensates for the gravitational torque $\beta = m_h g l_{cm} \cos(\theta)$ as in Equation (7) and plays a significant role in hovering the helicopter at the desired position. It can be expressed as:

$$u_{ff} = k_{ff} \frac{m_h g l_{cm} \cos(\theta)}{K_{PP}} \tag{15}$$

where $k_{ff}$ is the feed-forward control gain and is equal to 1.0 if it is to be considered; otherwise, it assumes a zero value.

### B. INTELLIGENT ACTIVE FORCE CONTROL (IAFC)

The AFC strategy is an effective method that basically depends on the appropriate estimation of the estimated inertia (or mass) of the system dynamics and the accurate measurements of the torque (or force) and acceleration signals of the physical system (plant) as shown in **Figure 4**. Therefore, the value of the estimated inertia plays a dominant role in improving the performance of the AFC strategy. It can be found using a crude approximation or intelligent methods [3].

In this work, the AFC parameter was obtained using artificial intelligence (AI) methods incorporating IL, and thus, it is defined as IAFC. The open-loop transfer function ($TF$) of the plant can be obtained by considering the following expression:

$$TF = \frac{\text{output}}{\text{input}} = \frac{\alpha}{T} \tag{16}$$

where

$T$ : torque applied to the system
$\alpha$ : angular acceleration

If the external disturbances are applied to the dynamic system, then:

$$TF = \frac{\alpha}{T + D} \tag{17}$$

Implementing the AFC strategy:

$$TF = \frac{\alpha}{U_T + D} = \frac{\alpha}{U + Q^* + D} \tag{18}$$

where

$U_T$ : total control output signal
$U$ : controller output signal
$D$ : disturbance applied to the system
$Q^*$ : AFC output signal such that:

$$Q^* = WF * D'$$

$D'$ : estimated disturbance torque
$WF$ : weighting function

$$D' = T' - I'\alpha' \tag{19}$$

where

$T'$ : measured torque
$I'$ : estimated mass moment of inertia
$\alpha'$ : measured angular acceleration

The superscript ($'$) means the measured, estimated, or computed parameters. $T'$ and $\alpha'$ are measurable quantities that can be measured using a torque sensor and an accelerometer, respectively. As a DC motor was assumed as the actuator, equation (19) can be expressed as:

$$D' = I_t K_t - I'\alpha' \tag{20}$$

where $I_t$ is the motor current and $K_t$ is the motor torque constant. In this study, iterative learning (IL), as an intelligent method, was employed for tuning the AFC strategy, which is demonstrated in the following sections.

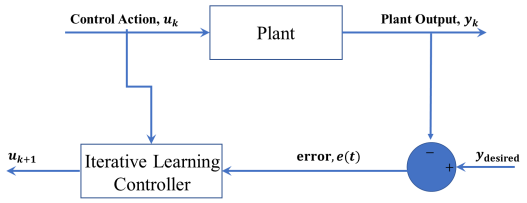


**FIGURE 5.** Schematic diagram of the ILC technique.

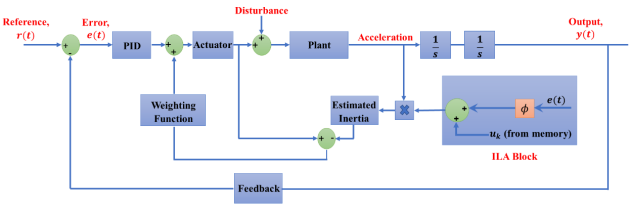


**FIGURE 6.** A schematic diagram of the PID-AFC-IL.

### C. ITERATIVE LEARNING CONTROL (ILC)

ILC is a type of adaptive intelligent control that acts smartly by emulating the function of human brain learning to enhance the automatic control systems and achieve better performance. It relies on improving the transient response of the dynamic systems that repeatedly operate over a fixed period [24]. It also enhances the system performance using the prior information of the previous iterations [25]. It is essential to implement an algorithm to generate the next control input in such a way that the error is gradually reduced or converged on successive trails. Due to the similarity of the mathematical expression associated with the classical PID controller, the IL algorithm could be duly described as P, PI, PD, or PID-type ILC algorithm [24], as shown in **Figure 5**. The ILC algorithm was applied to a TRMS model in [26] to achieve desired conditions while performing the trajectory tracking task as results demonstrated the ability of the ILC in improving system performance efficiently.

The learning control rule for a PID-type can be expressed mathematically as [24]:

$$u_{k+1}(t) = u_k(t) + Ke_k(t) \tag{21}$$

where

$u_{k+1}(t)$ : next step input
$u_k(t)$ : current input
$e_k(t)$ : current error
$K$ : designed parameter (constant) containing the PID term:

$$K = \phi + \Gamma \int dt + \psi \frac{d}{dt} \tag{22}$$

$\phi$, $\Gamma$, and $\psi$: learning constants related to the P, I, and D terms, respectively

### D. PROPOSED PID-AFC-IL CONTROL SYSTEM

In this study, we propose a hybrid control scheme comprising the PID controller integrated with the AFC strategy tuned using the IL algorithm embedded into the AFC loop. A P-type IL algorithm was developed for the experimental work for its simplicity in real-time implementation to compute the appropriate value of the estimated inertia matrix ($IM$) automatically while on-line, according to:

$$IM_{k+1} = IM_k + Ke_k(t) \tag{23}$$

where

$IM_{k+1}$ : next step estimated inertia
$IM_k$ : current estimated inertia
$K = \phi$ : P-type learning constant

For the P-type IL algorithm, both the input and output signals were stored in memory each time the system operates. The next input signal was computed in such a way the IL algorithm will force the performance error to be reduced in the subsequent iteration, a process very similar to the classic PID control algorithm. The objective of the IL algorithm is to update the value of the estimated inertia iteratively, and the error is expected to converge to a value approaching the zero datum. The schematic block diagram of the PID-AFC-IL is shown in **Figure 6**.

Moreover, for the stability analysis of the PID-AFC scheme, it was proven that the stability of the control system is independent of the 2-DOF helicopter model; however, it just depends on the actuator dynamics, PID parameters, and estimated inertia of the AFC strategy. Thus, the stability condition of the 2-DOF helicopter model will not affect the stability of the whole system. Additionally, this guarantees that the system displays responses that are limited when excited with proper inputs to the system [27].

## IV. EXPERIMENTAL SETUP

An experimental test rig was designed and developed for the twin-rotor helicopter model to evaluate the effectiveness of the proposed IAFC-based controller in rejecting the applied disturbances. Basically, to improve the effectiveness of the AFC strategy, the proper selection of the estimated inertia ($I$) is deemed crucial to compensate for the external disturbances successfully. The estimated inertia can be obtained using the crude approximation method [21] or utilizing intelligent means [3]. In this research, the self-tuning (ST) AFC employing an IL algorithm method combined with a conventional PID controller, known as the PID-AFC-IL scheme, was proposed. The IL algorithm features ease of implementation and efficiency to reach optimum inertial values automatically and on-line. For this purpose, a full mechatronic approach was adopted for the experimental test rig to integrate all the related elements synergistically.

The dual-rotor model being a mechatronic system, constitutes the mechanical, electrical/electronic, and computer control components, as shown in **Figure 7**. Firstly, the mechanical sub-system comprising the mechanical parts that were deliberately designed and developed to execute certain physical motions. The electrical and electronic components involving the actuators and sensors were operated via signal conditioning and interface/driver circuits based on the physical aspects of the twin-rotor model and its assembly. Lastly, the computer control includes programming of the

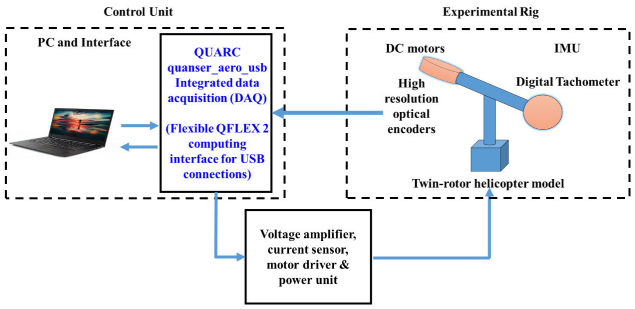


**FIGURE 7.** A schematic configuration of the mechatronic system.

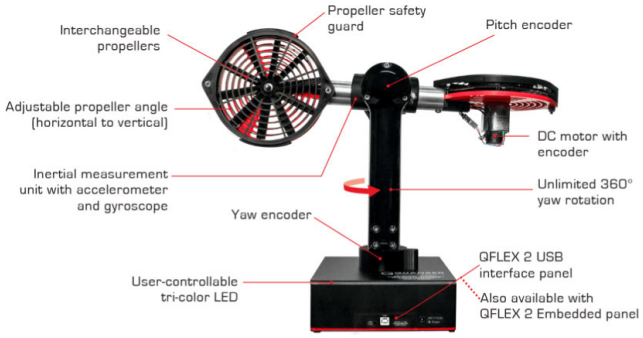


**FIGURE 8.** *Quanser Aero* apparatus [28].

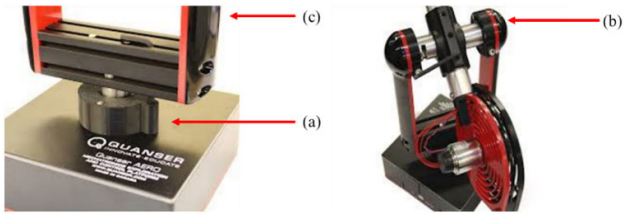


**FIGURE 9.** (a) Yaw pivot (b) Pitch pivot (c) Support yolk [28].

**TABLE 1.** The main *Quanser Aero* components [29].

| Description | Symbol | Value |
|---|---|---|
| Mass of body | $M_b$ | 1.075 kg |
| Center of mass | $D_m$ | -7.59 mm |
| Pitch inertia | $J_P$ | $2.15 \times 10^{-2}$ kgm$^2$ |
| Yaw inertia | $J_y$ | $2.37 \times 10^{-2}$ kgm$^2$ |
| Thrust displacement | $D_t$ | 15.8 cm |
| Drag/Air resistance coefficient | $k_d$ | $1 \times 10^{-5}$ Nm/(rad/s) |
| Propeller hub inertia | $J_h$ | $3.04 \times 10^{-9}$ kgm$^2$ |
| Propeller inertia | $J_p$ | $7.2 \times 10^{-6}$ kgm$^2$ |

input/output (I/O) devices in MATLAB/Simulink to control the 2-DOF helicopter system according to the desired mission via the proposed hybrid control scheme.

In this study, the *Quanser Aero* apparatus was utilized as the main test rig platform for the experimental study. It is a fully integrated TRMS laboratory experimental module, as shown in **Figure 8**. In the following sections, the detailed experimental set-up was demonstrated.

### A. EXPERIMENTAL TEST RIG

#### 1) SYSTEM DESCRIPTION AND MECHANICAL COMPONENTS

The *Quanser Aero* is a 2-DOF twin-rotor laboratory experimental module. It is the off-the-shelf version deemed the most suitable device for describing a helicopter system precisely and rotorcraft UAV generally. It consists of two propellers with ten vanes, each rotating opposite to each other (counter-rotating) and a guard (housing) to protect them from colliding with obstacles. The front rotor, *Thruster 0*, positioned parallel to the ground, is considered the main rotor and causes a pitching moment around the pitch axis. The back or tail rotor, *Thruster 1*, generates a yawing moment around the yaw axis. The pitching angle is bounded by ±62° from the horizontal position due to physical limits in the apparatus, while the yaw angle can rotate freely, i.e., 360° without any constraints. The propeller diameter is 12.7 cm and both the 3-D printed propellers fixed at both ends of a beam are driven by two coreless DC motors that use aluminum prop adaptors with collets (propellers hubs) – the model assembly is *EFLM1922*. There are two pivots; namely, the pitch pivot that allows the rotation freely in the vertical plane and the yaw pivot which allows the rotation freely about the horizontal plane as depicted in **Figures 9 (a)** and **(b)**. The beam pivoted on its fixed base through a support yolk as shown in **Figure 9 (c)**. The base dimensions are 17.8 cm × 17.8 cm × 7 cm where the device height with propellers in a horizontal position is 35.6 cm. The length of the *Quanser Aero* device is 51 cm whereas its mass is 3.6 kg. The parameter specifications of the *Quanser Aero* are shown in **Table 1**.

#### 2) ELECTRICAL/ELECTRONIC COMPONENTS AND COMPUTER CONTROL

The electrical/electronic components primarily make up the signal conditioning and interface circuits to perform various functions, including amplifying, computing, and transferring the control signal of the electrical-based devices. The I/O interface board is the link between the electro-mechanical components and the personal computer (PC). It provides analog-to-digital and digital-to-analog conversions, as shown in **Figure 10**, using the *Quanser Aero* USB board (hardware) and *Quanser* Real-Time Control Software (*QUARC*) as the driver. The *Quanser Aero* provides two different types of I/O interface panels, namely, the *QFLEX 2 USB* and *QFLEX 2 Embedded*. The *QFLEX 2 USB* provides a USB interface for computer usage. In contrast, the *QFLEX 2 Embedded* provides a 4-wire serial peripheral interface (SPI) for external microcontroller boards such as *myRIO*, *Arduino,* or *Raspberry Pi*. In this study, *QFLEX 2 USB* was employed to be interfaced with the PC/laptop via the USB connection.

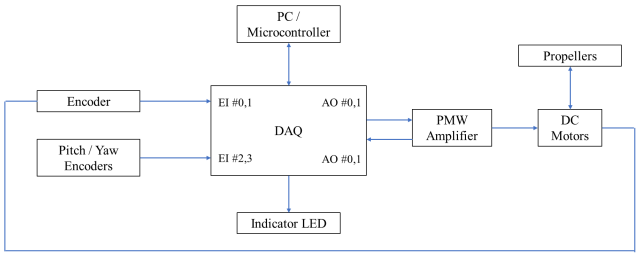


**FIGURE 10.** The link between *Quanser Aero* components [28].

The *Quanser Aero* module includes an integrated data acquisition (DAQ) device with four 16-bit encoder channels with quadrature decoding and two pulse-width modulations (PWM) analog output channels. Also, it incorporates a 12-bit analog-digital converter (ADC) to provide the current sense feedback for the motors to prevent the motor from stalling and stop the amplifier if a stall is detected. The module also includes two types of built-in optical encoders. The first type was used to measure the pitch and angular position of the DC motors, where it outputs 2048 counts per revolution in quadrature (or 512 cycles per rev (CPR)). While the other is used to measure the yaw of the support yolk, where its output is 4096 counts per revolution in quadrature (or 1024 CPR). The encoder type for the pitch and DC motors are *US Digital E8P-512-118* single-ended optical shaft encoder, while the encoder for yaw is *US Digital E3-1024-984*. The angular position signal was first picked by the encoder and later sent to the PC via the DAQ system and amplifier.

A power amplifier is usually needed to increase the magnitude of the power of the signal and drive the DC motors via computer control. The *Quanser Aero* includes a built-in PWM voltage-controlled power amplifier to provide a 2 A peak current and 0.5 A continuous current (based on the thermal current rating of the motor). The output voltage range to the load is $\pm 24$ V.

A DC motor was used to drive the propellers. The proper selection of the motor was mainly based on the amount of torque required to drive the propeller, considering the physical masses, loads, and external disturbances. The *Quanser Aero* includes two direct-drive brushed DC motors types based on *Allied Motion CL40* series coreless DC motor model, *16705*. The complete specifications of the motor are listed in **Table 2**. The DC motor maximizes its performance by utilizing high-performance permanent magnets, a uniquely wound, formed coreless rotor, and a precious-metal communication system. This type is characterized by no cogging and iron loss, high strength magnets, low starting voltages, and low rotor inertia leading to rapid responses, smooth speeds, high-efficiency operations, and cog-free operations. The necessary relationships of the motor that was used in this study are given as:

$$\tau_{\mathrm{m}} = J_{\mathrm{eq}} \dot{\omega}_{\mathrm{m}}(t) \tag{24}$$

$$\tau_{\mathrm{m}} = K_{\mathrm{t}} i_{\mathrm{m}}(t) \tag{25}$$

**TABLE 2.** Coreless DC motor model 16705 specifications [29].

| Parameter | Symbol | Value |
|---|---|---|
| Nominal input voltage | $V_{\mathrm{nom}}$ | 18 V |
| Nominal torque | $\tau_{\mathrm{nom}}$ | 22 mNm |
| Nominal speed | $\omega_{\mathrm{nom}}$ | 3050 rpm |
| Nominal current | $I_{\mathrm{nom}}$ | 0.54 A |
| Terminal resistance | $R_{\mathrm{m}}$ | 8.4 Ohm |
| Torque constant | $K_{\mathrm{t}}$ | 0.042 N m/A |
| Motor back-emf constant | $K_{\mathrm{m}}$ | 0.042 V/(rad/s) |
| Rotor inertia | $J_{\mathrm{m}}$ | $4 \times 10^{-6}$ kg m$^2$ |
| Rotor inductance | $L_{\mathrm{m}}$ | 1.16 mH |

where

$\tau_{\mathrm{m}}$ : motor torque
$J_{\mathrm{eq}}$ : total moment of inertia acting on the motor shaft
$\dot{\omega}_{\mathrm{m}}(t)$ : angular acceleration
$K_{\mathrm{t}}$ : torque constant
$i_{\mathrm{m}}(t)$ : motor current

Based on *Kirchoff's* voltage law, and the motor inductance $L_{\mathrm{m}}$ is much less than its resistance $R_{\mathrm{m}}$ (can be safely ignored), the motor current can be found as:

$$i_{\mathrm{m}}(t) = \frac{v_{\mathrm{m}}(t) - K_m \omega_{\mathrm{m}}(t)}{R_{\mathrm{m}}} \tag{26}$$

where

$v_{\mathrm{m}}(t)$ : motor input voltage
$K_m$ : motor back-emf constant
$\omega_{\mathrm{m}}(t)$ : motor speed
$R_{\mathrm{m}}$ : motor resistance

There must be a saturation limit to the motor voltage output so that it should not be exceeded during the operation. Otherwise, it may cause severe damage to the DC motors. Therefore, a saturation block was utilized in the Simulink block diagram where the maximum and minimum limits were set to be $\pm 24$ V. Any output value exceeding these limits will be reset to either a maximum $+24$ V or minimum $-24$ V.

For real-time measurement of the linear and angular motions along with all the three primary axes, the *Quanser Aero* includes a built-in inertial measurement unit (IMU) fixed within the body, which is *STMicroelectronics LSM6DS0 iNEMO* inertial module. It features a 3D digital gyroscope and a 3D digital accelerometer providing performance at 0.55 mA in high-performance mode and allowing always-on low-power features for an optimal motion experience. For this work, the required angular acceleration can be obtained either using direct differentiation with a low pass filter of the angular velocity acquired from the tachometer sensor signal or using Equation (24). The low pass filter was used to remove the unwanted noise of the output signal where the cut-off frequency is 100 rad/s.

The computer control includes programming of the I/O board to achieve the desired/reference pitch or yaw positions. It was used to control the twin-rotor helicopter model

**TABLE 3.** PID controller parameters for the step input.

| PID parameters | Value |
|---|---|
| Proportional gain, $K_P$ | 100 |
| Integral gain, $K_I$ | 35 |
| Derivative gain, $K_D$ | 85 |
| Cut-off frequency, $\omega_n$ (rad/s) | 100 |

**TABLE 4.** PID controller parameters for the pulsating input.

| PID parameters | Value |
|---|---|
| Proportional gain, $K_P$ | 200 |
| Integral gain, $K_I$ | 92 |
| Derivative gain, $K_D$ | 150 |
| Cut-off frequency, $\omega_n$ (rad/s) | 150 |

according to the required mission via the proposed control scheme using the *QUARC* software driver. It was seamlessly integrated with MATLAB/Simulink and enabled the Simulink models to be executed in real-time. The *QUARC* further adds powerful tools and capabilities in MATLAB/Simulink environment and, in turn, greatly facilitates the development of sophisticated mechatronic and control applications in real-time.

### B. EXPERIMENTAL PARAMETER SETTINGS AND INITIAL CONDITIONS

Three types of control schemes were implemented - the classical PID followed by the PID-AFC and finally the PID-AFC-IL control strategies. Firstly, the PID controller was designed with its gains heuristically adjusted for both the step and pulsating references, as shown in **Tables 3** and **4**, utilizing a sampling rate of 1 ms. For the AFC strategy, the estimated inertia was assumed to be fixed and having an overestimated value, i.e., $I > J_{eq}$ to give sufficient stability conditions [3]. In this work, the estimated inertia was obtained using two approaches, namely, the crude approximation (PID-AFC) and the iterative learning algorithm (PID-AFC-IL). In the first strategy, the value of the $I$ was pre-assigned with a fixed value of 0.05 kgm$^2$, while for the latter, no prior knowledge of the value of $I$ was needed. The learning algorithm used was a P-type IL with an initial condition of $I$ set to 0.07 kgm$^2$ and learning parameter ($\Phi$) heuristically assigned as 0.000001. It is worth noting that desirable advantages of the designed control strategy are its flexibility and its ease in producing the smooth switching of the control actions from the P, PI, PD, or PID controllers to the AFC-based controller by systematically manipulating the PID gains and exploiting a set of a simple slider and switching mechanism within the Simulink environment.

In this experiment, two types of reference or input trajectories were chosen - the step and pulsating signals, as shown in **Figure 11**. The step input was started at a step time of 1 s wherein its steady-state angular displacement was 20°. The pulsating input was set with an amplitude of ±10° at a 5 s interval. The external disturbance was firstly disregarded, but later, they were applied to the helicopter system to test the effectiveness of the proposed control schemes in tracking the reference trajectory and eliminating the applied disturbances. Regarding the external disturbances applied to the dual-rotor helicopter system, two types were introduced, namely, the impulsive force and payload mass disturbances. The impulsive force was applied at approximately 10 s from the start of the operation. In contrast, the other disturbance type is in the form of a 7 g payload mass inserted approximately 10 seconds after starting the process. For simplicity, the yaw of the yoke was locked so the pitch motion was only considered to transform the double-rotor helicopter system effectively into a 1-DOF system.

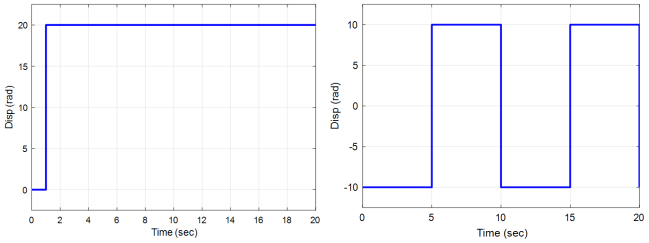


**FIGURE 11.** Types of input trajectories (a) step and (b) pulsating.

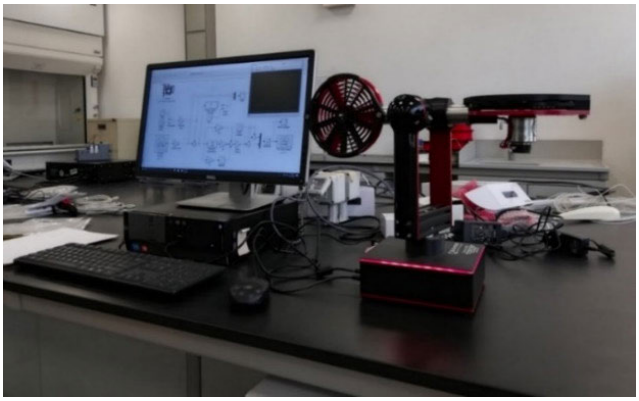

**FIGURE 12.** A view of the dual rotor helicopter model experimental rig.

A view of the 2-DOF helicopter experimental test rig is shown in **Figure 12**. While, the Simulink block diagram of the helicopter system with the PID, PID-AFC, and PID-AFC-IL control strategies is shown in **Figure 13**.

The design procedures for the proposed IAFC scheme (the green block in **Figure 13**) are based on equation (20) without assigning any preset value of $I$. The logic of the P-type IL algorithm (the red block in **Figure 13**) employed for the IAFC approach, to find the value of I intelligently, is described in a flowchart indicated in **Figure 14**. A discrete state-space block was utilized for the IL model to represent a portion of the algorithm. The model receives the error as the input, which is

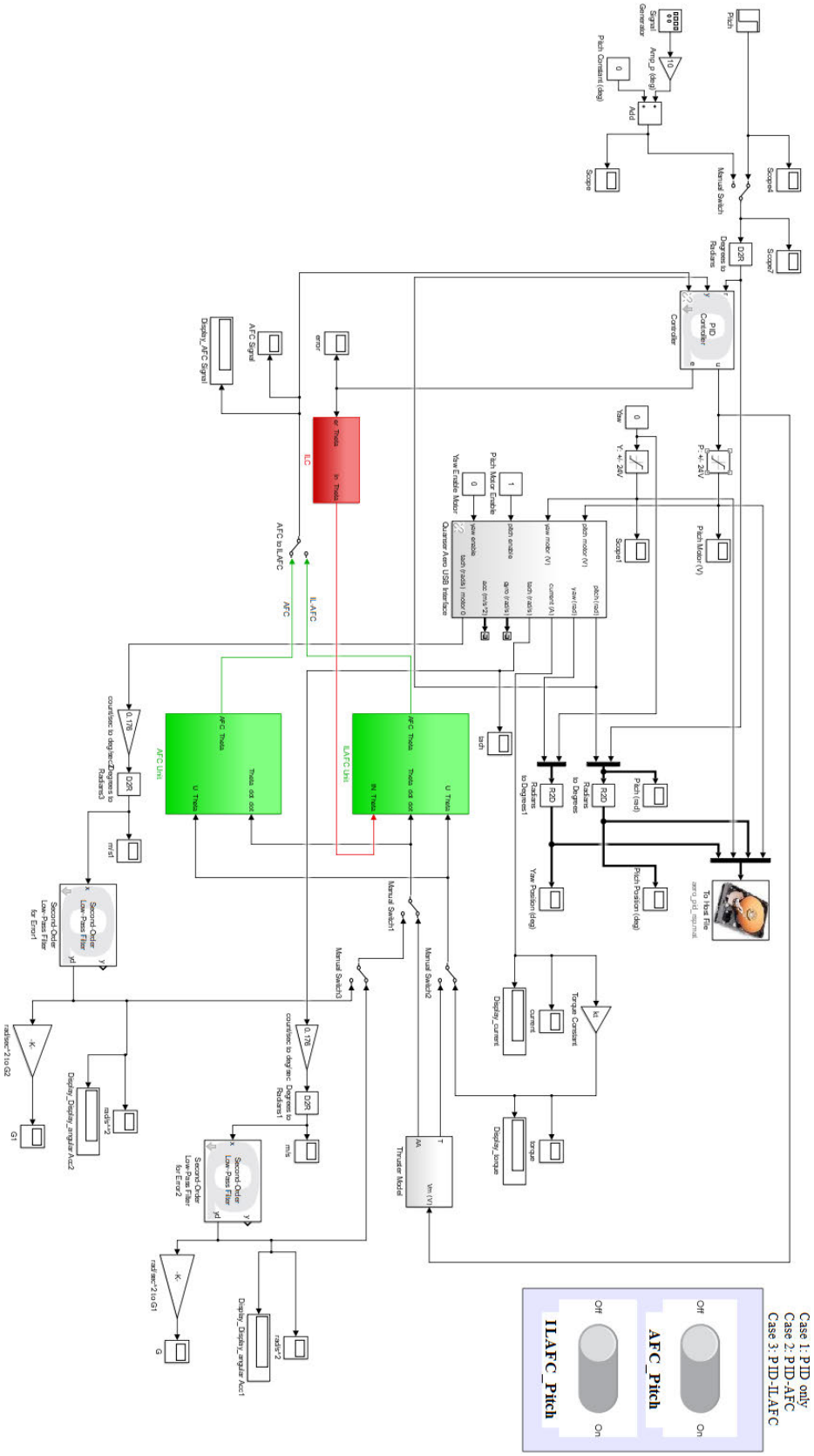


**FIGURE 13.** Simulink block diagram of the twin-rotor helicopter system with PID, PID-AFC, and PID-AFC-IL control schemes.

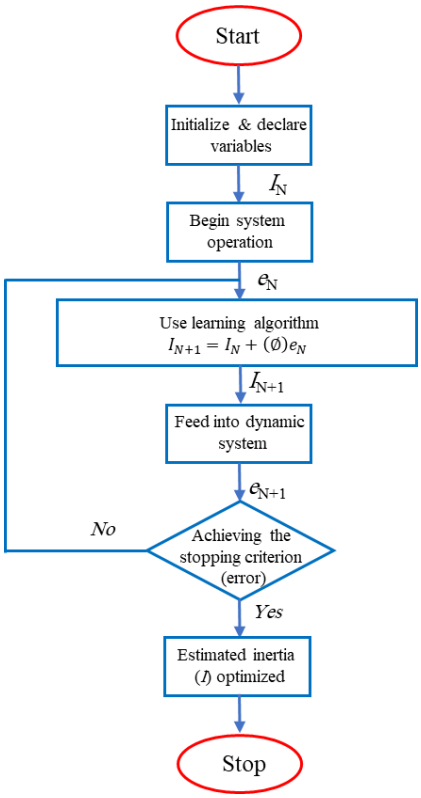


**FIGURE 14.** A flowchart illustrating the proposed P-type IL algorithm.

processed by the iterative learning algorithm, and the desired *IM* as the output from the model, which is fed into the IAFC block of **Figure 13**.

The experimental results were divided into two scenarios; the first was to study the behavior of the 2-DOF helicopter system with the step-input trajectory, while the other is related to the pulsating trajectory. In each scenario, three cases were studied, namely, without any disturbances, with the presence of an impulsive force, and finally considering the applied payload mass disturbance. In each case, a comparison of the proposed PID, PID-AFC, and PID-AFC-IL controllers was performed in the time domain, and the ensuing results are described in the following paragraphs.

## V. RESULTS AND DISCUSSION

### A. FIRST SCENARIO: STEP-INPUT TRAJECTORY

In this scenario, the behavior of the twin-rotor helicopter system against the step input was analyzed. Additionally, the effectiveness of the AFC-based controllers was assessed and compared to the PID controller under different conditions as described in the following cases:

*Case 1:* Without any disturbances

The response of the trajectory tracking of the twin-rotor helicopter system against a step input and without applying any type of external disturbances is shown in **Figure 15**. In contrast, the current and angular acceleration responses are shown in **Figure 16**. The results are based on the three types of controllers related to the PID, PID-AFC, and PID-AFC-IL.

**TABLE 5.** RMSE of the control strategies with various disturbances.

| | RMSE | | | | | |
|---|---|---|---|---|---|---|
| | Step input | | | Pulsating input | | |
| | PID | PID-AFC | PID-AFC-IL | PID | PID-AFC | PID-AFC-IL |
| Without disturbances | 33.73 | 26.60 | 24.54 | 8.84 | 7.40 | 6.94 |
| | PID | | PID-AFC-IL | PID | | PID-AFC-IL |
| Impulsive force | 35.69 | | 26.02 | 10.87 | | 9.43 |
| Payload mass | 34.62 | | 25.34 | 22.78 | | 17.48 |

It can be clearly seen that the best results are obtained for the AFC-based control strategies though the differences are slight and relatively marginal.

*Case 2:* With impulsive force disturbance

In this case, an impulsive force was applied to the double-rotor helicopter model to study the effectiveness of the proposed control schemes in rejecting the applied disturbances. Based on previous findings in *Case 1*, the results indicated that the PID-AFC-IL strategy performs better than the PID-AFC scheme; thus, the remaining cases in the first scenario were between the PID and PID-AFC-IL schemes. **Figure 17** shows the responses of the current and angular acceleration for the pitching motion.

*Case 3:* With payload mass disturbance

In this case, a payload mass disturbance was applied to the helicopter system to study the effectiveness of the PID and PID-AFC-IL schemes. The current and angular acceleration responses are shown in **Figure 18**.

### B. SECOND SCENARIO: PULSATING INPUT TRAJECTORY

In this scenario, the behavior of the 2-DOF dual-rotor helicopter system against the pulsating input was studied. Moreover, the efficacy of the AFC-based controllers was examined and compared to the PID controller as described in the following cases:

*Case 1:* Disturbances disregarded

The trajectory tracking behavior of the double-rotor model against pulsating input and without applying any type of disturbances is shown in **Figure 19**. In contrast, the current and angular acceleration responses are shown in **Figure 20**.

*Case 2:* With impulsive force disturbance

In this case, the impulsive force disturbance was introduced to the twin-rotor platform to study the effectiveness of the proposed control schemes, as shown in **Figure 21**.

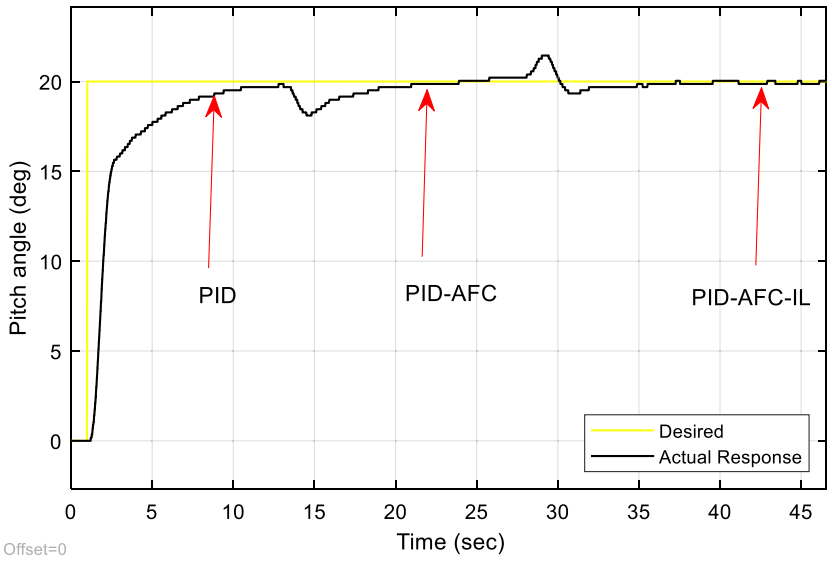


**FIGURE 15.** Superimposed results of the control schemes for a given step input.

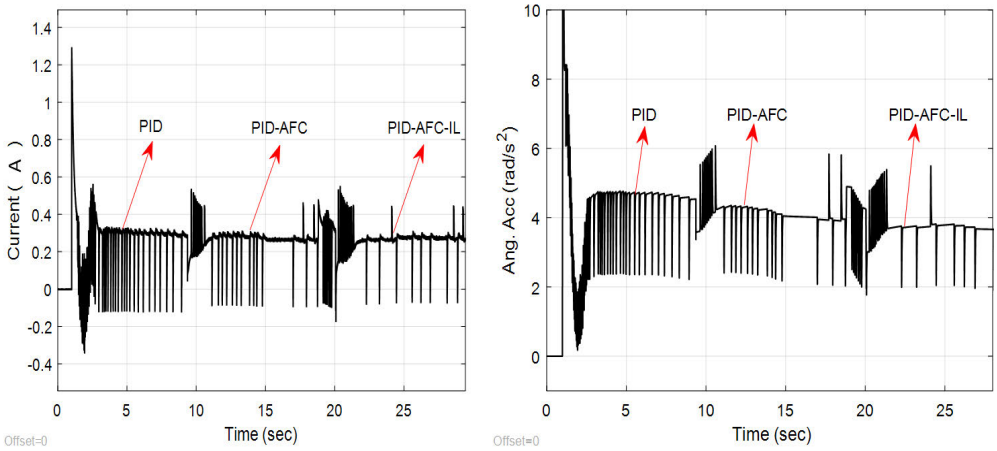


**FIGURE 16.** Current and angular acceleration responses without any disturbances.

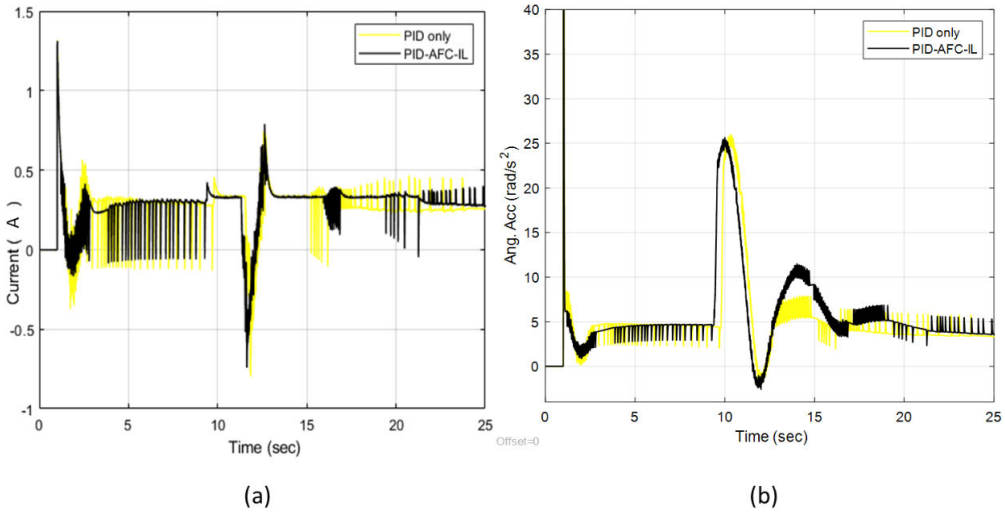


**FIGURE 17.** Current and angular acceleration responses for impulsive force disturbance.

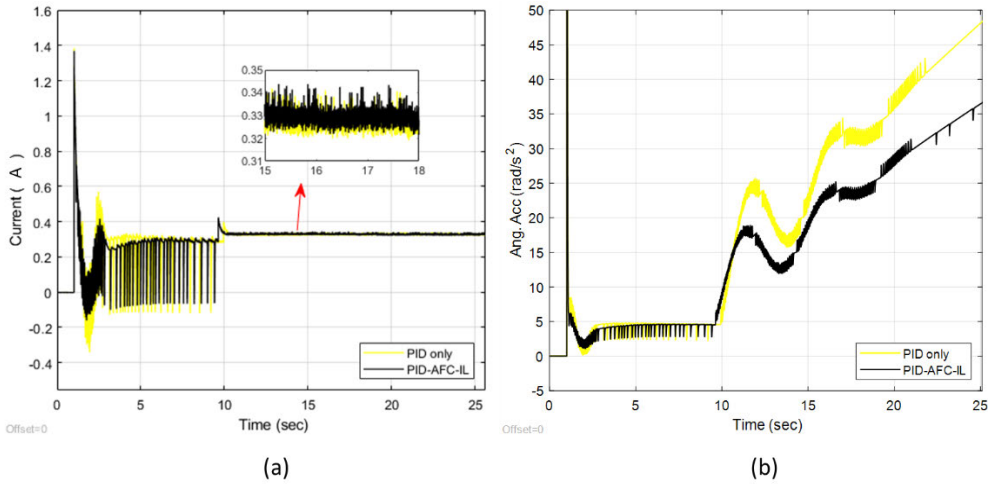


**FIGURE 18.** Current and angular acceleration responses for payload mass disturbance.

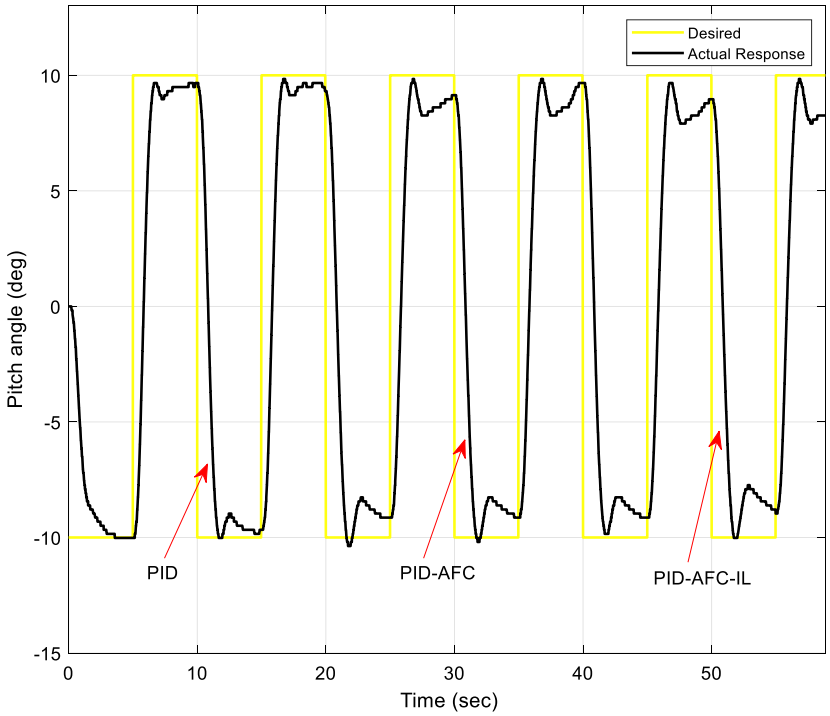


**FIGURE 19.** Superimposed results of the control schemes for a given pulsating input.

*Case 3:* With payload mass disturbance

The payload mass disturbance was applied to the TRMS to study the efficacy of the PID and PID-AFC-IL control schemes, as shown in **Figure 22**.

It can be observed from **Figures 15** and **19** that all the proposed control schemes follow the reference trajectory despite the presence of some noises due to the nature of the real-time implementation environment. The results in **Figure 19** also revealed a rapid response with some acceptable overshoots and some minor steady-state errors when using the suggested AFC-based control strategies in the case of the pulsating reference. Meanwhile, for **Figures 16** and **20**, better efficacy of the IAFC-based scheme can be inferred, showing the best overall performance compared to the other control structures.

Also, the experimental results indicated better effectiveness of the proposed IAFC-based controller in the presence of impulsive force and payload mass disturbances compared to the PID controller. It is evident that the PID-AFC-IL strategy shows better performance in terms of the current and angular acceleration responses. In other words, the IAFC-based

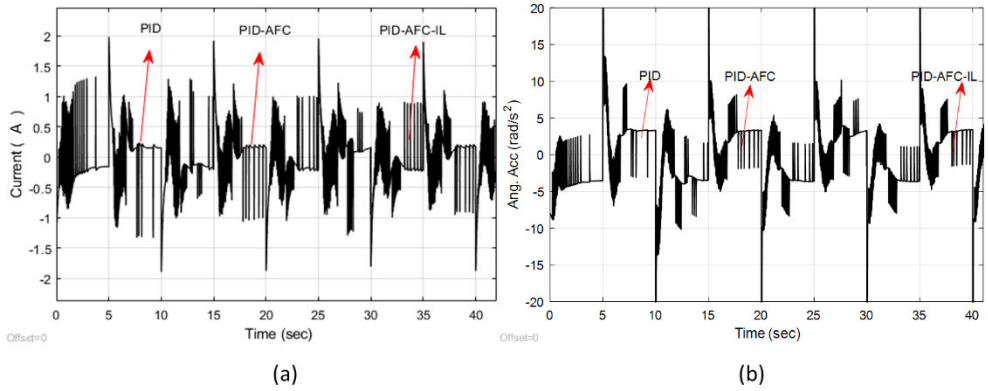


**FIGURE 20.** Current and angular acceleration responses without any disturbances.

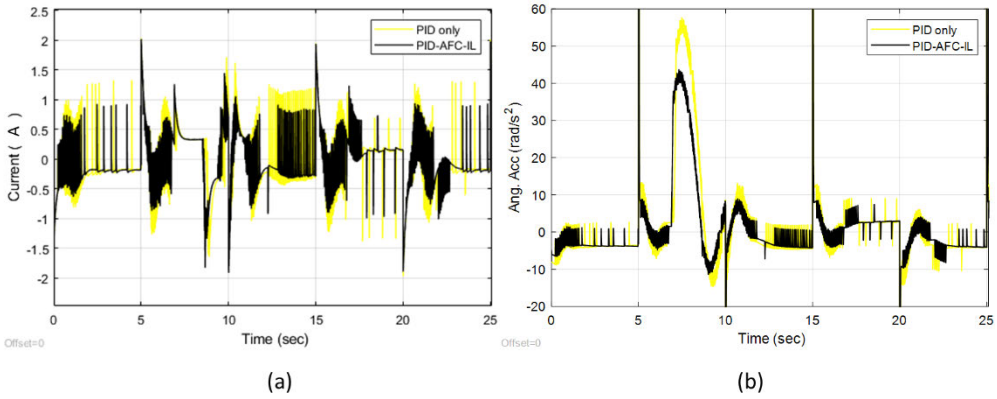


**FIGURE 21.** Current and angular acceleration responses for impulsive force disturbance.

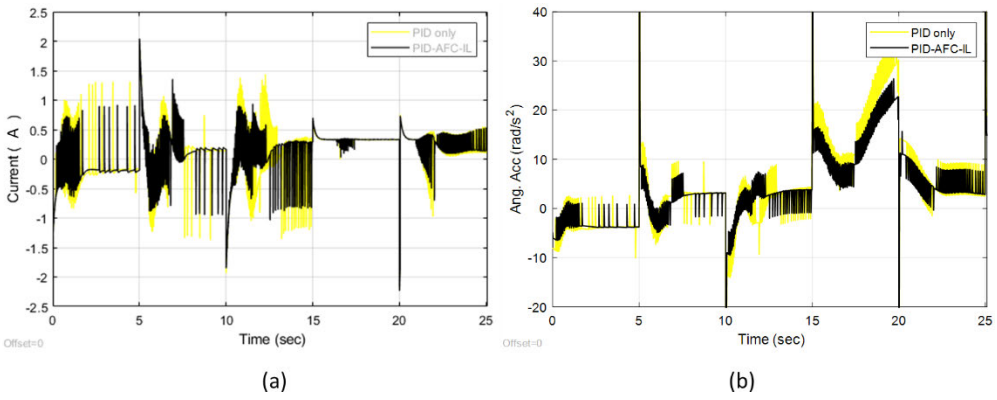


**FIGURE 22.** Current and angular acceleration responses for payload mass disturbance.

control scheme is able to enhance the system performance and disturbance rejection capability. Moreover, the experimental results show the effectiveness of the iterative learning algorithm in optimizing the estimated inertia values automatically while on-line. In this study, to assess the improvement in system performance and present the performance measures of the proposed IAFC scheme with regard to other methods, the root mean square error (RMSE) values of output signals were employed to deduce the best result. The RMSE can be expressed as:

$$\mathrm{RMSE} = \sqrt{\frac{1}{N}\sum_{i=1}^{N}[x_i]^2} \tag{27}$$

where $N$ is the sample size and $x_i$ the output signal.

The RMSE for a number of responses is listed in **Table 5**. It can be seen that the lower the RMSE value, the more effective the proposed control strategy. The percentages of

improvements in the system performance based on the RMSE were calculated with the PID control scheme considered as the reference base for comparison.

It can be seen from **Table 5** that the PID-AFC-IL strategy showed superior efficiency compared to other controllers based on the RMS error values. Meanwhile, the percentages of improvements in the performance based on the PID-AFC and PID-AFC-IL schemes in the absence of disturbances are 21.1% and 27.2%, respectively, for the step input trajectory and 16.2% and 21.5%, respectively for the pulsating input trajectory. Moreover, it can be concluded that in the presence of the impulsive force disturbance, the percentages of improvement in the system performance for the PID-AFC-IL are 27% and 13.2% for the step and pulsating input trajectories. In contrast, in the presence of the payload mass disturbance, the improvements are 26.8% and 23.2%, respectively.

## VI. CONCLUSION

The proposed PID-AFC-IL scheme representing an IAFC-based controller has been successfully designed and implemented to a twin-rotor system. The system behavior and effectiveness have been numerically analyzed and benchmarked with the designed PID-AFC and PID control systems. The AFC-based control schemes clearly demonstrate the robust performance in stabilizing the UAV and rejecting the different types of introduced disturbances, in comparison to the other control scheme counterpart. The effectiveness of the practical implementation of the IAFC-based controller on the twin-rotor helicopter system, as a model of rotorcraft UAVs, has been duly verified and validated. The 2-DOF dual rotor model test rig has been developed and experimented with, considering several terrain profiles and disturbances.

The experimental results revealed the effectiveness of the PID-AFC-IL strategy in producing the best efficacy (lowest RMSE) compared to the other control approaches. In addition, the practical results showed good agreement with the previously simulated results. About 27% improvement in system performance was observed for both disturbance conditions based on the RMSE analysis. Future work may include different operating and loading conditions to illustrate the feasibility and testify the robustness of the proposed control strategy. Moreover, the real-time implementation of the suggested control strategies may be addressed, focusing more on the non-linear properties, coupling characteristics, and the effect of parameter variations on the dynamic response of the helicopter system, while adding more comparative results, possibly including a fuzzy logic-based active force control strategy.

## REFERENCES

[1] Y. Xin, Z.-C. Qin, and J.-Q. Sun, "Input-output tracking control of a 2-DOF laboratory helicopter with improved algebraic differential estimation," *Mech. Syst. Signal Process.*, vol. 116, pp. 843–857, Feb. 2019, doi: 10.1016/j.ymssp.2018.07.027.

[2] S. K. Pandey, J. Dey, and S. Banerjee, "Design of robust proportional–integral–derivative controller for generalized decoupled twin rotor multi-input-multi-output system with actuator non-linearity," *Proc. Inst. Mech. Eng., I, J. Syst. Control Eng.*, vol. 232, no. 8, pp. 971–982, Aug. 2018, doi: 10.1177/0959651818771487.

[3] M. Mailah, *Intelligent Active Force Control of a Rigid Robot Arm Using Neural Network and Iterative Learning Algorithms*. Dundee, Scotland: Univ. Dundee, 1998.

[4] S. Ijaz, M. T. Hamayun, L. Yan, and M. F. Mumtaz, "Fractional order modeling and control of twin rotor aero dynamical system using nelder mead optimization," *J. Electr. Eng. Technol.*, vol. 11, no. 6, pp. 1863–1871, Nov. 2016.

[5] H. Ali, A. Ali, and I. U. H. Shaikh, "Disturbance observer based control of twin rotor aerodynamic system," *Turkish J. Elect. Eng. Comput. Sci.*, vol. 28, no. 4, pp. 2213–2227, Jul. 2020.

[6] M. Witczak, M. Buciakowski, V. Puig, D. Rotondo, and F. Nejjari, "An LMI approach to robust fault estimation for a class of nonlinear systems," *Int. J. Robust Nonlinear Control*, vol. 26, no. 7, pp. 1530–1548, May 2016, doi: 10.1002/rnc.3365.

[7] H. Rojas-Cubides, J. Cortés-Romero, H. Coral-Enriquez, and H. Rojas-Cubides, "Sliding mode control assisted by GPI observers for tracking tasks of a nonlinear multivariable twin-rotor aerodynamical system," *Control Eng. Pract.*, vol. 88, pp. 1–15, Jul. 2019, doi: 10.1016/j.conengprac.2019.04.002.

[8] F. Faris, A. Moussaoui, B. Djamel, and T. Mohammed, "Design and real-time implementation of a decentralized sliding mode controller for twin rotor multi-input multi-output system," *Proc. Inst. Mech. Eng., I, J. Syst. Control Eng.*, vol. 231, no. 1, pp. 3–13, Jan. 2017, doi: 10.1177/0959651816680457.

[9] R. Rashad, A. El-Badawy, and A. Aboudonia, "Sliding mode disturbance observer-based control of a twin rotor MIMO system," *ISA Trans.*, vol. 69, pp. 166–174, Jul. 2017, doi: 10.1016/j.isatra.2017.04.013.

[10] M. Ilyas, N. Abbas, M. UbaidUllah, W. A. Imtiaz, M. A. Q. Shah, and K. Mahmood, "Control Law Design for Twin Rotor MIMO System with Nonlinear Control Strategy," *Discrete Dyn. Nature Soc.*, vol. 2016, Art. no. 2952738, p. 2016, doi: 10.1155/2016/2952738.

[11] R. Raghavan and S. Thomas, "Practically implementable model predictive controller for a twin rotor multi-input multi-output system," *J. Control, Autom. Electr. Syst.*, vol. 28, no. 3, pp. 358–370, Jun. 2017, doi: 10.1007/s40313-017-0311-5.

[12] S. Zeghlache and N. Amardjia, "Real time implementation of non linear observer-based fuzzy sliding mode controller for a twin rotor multi-input multi-output system (TRMS)," *Optik*, vol. 156, pp. 391–407, Mar. 2018, doi: 10.1016/j.ijleo.2017.11.053.

[13] A. A. Najm and I. K. Ibraheem, "Altitude and attitude stabilization of UAV quadrotor system using improved active disturbance rejection control," *Arabian J. Sci. Eng.*, vol. 45, no. 3, pp. 1985–1999, Mar. 2020, doi: 10.1007/s13369-020-04355-3.

[14] X. Yang, J. Cui, D. Lao, D. Li, and J. Chen, "Input shaping enhanced active disturbance rejection control for a twin rotor multi-input multi-output system (TRMS)," *ISA Trans.*, vol. 62, pp. 287–298, May 2016, doi: 10.1016/j.isatra.2016.02.001.

[15] J. R. Hewit and J. S. Burdess, "Fast dynamic decoupled control for robotics, using active force control," *Mechanism Mach. Theory*, vol. 16, no. 5, pp. 535–542, Jan. 1981, doi: 10.1016/0094-114X(81)90025-2.

[16] M. Tahmasebi, M. Gohari, M. Mailah, and R. Abd Rahman, "Vibration suppression of sprayer boom structure using active torque control and iterative learning. Part II: Experimental implementation," *J. Vibrat. Control*, vol. 24, no. 20, pp. 4740–4750, Oct. 2017, doi: 10.1177/1077546317733907.

[17] S. K. Badar Sharif and M. Mailah, "Real-time implementation of feed rate active force control of a syringe fluid dispenser," *Jurnal Teknologi*, vol. 79, no. 5, pp. 117–123, Jun. 2017, doi: 10.11113/jt.v79.10527.

[18] S. I. Abdelmaksoud, M. Mailah, and A. M. Abdallah, "Control strategies and novel techniques for autonomous rotorcraft unmanned aerial vehicles: A review," *IEEE Access*, vol. 8, pp. 195142–195169, 2020, doi: 10.1109/ACCESS.2020.3031326.

[19] M. S. Meon, T. L. T. Mohamed, M. H. M. Ramli, M. Z. Mohamed, and N. F. A. Manan, "Review and current study on new approach using PID active force control (PIDAFC) of twin rotor multi input multi output system (TRMS)," in *Proc. IEEE Symp. Humanities, Sci. Eng. Res.*, Jun. 2012, pp. 163–167, doi: 10.1109/SHUSER.2012.6268848.

[20] H. Ramli, W. Kuntjoro, M. S. Meon, and K. M. A. K. Ishak, "Adaptive active force control application to twin rotor MIMO system," *Appl. Mech. Mater.*, vol. 393, pp. 688–693, Sep. 2013, doi: 10.4028/www.scientific.net/AMM.393.688.

[21] M. Omar, M. Mailah, and S. I. Abdelmaksoud, "Robust active force control of a quadcopter," *Jurnal Mekanikal*, vol. 40, no. 2, pp. 12–22, Dec. 2017.

[22] S. I. Abdelmaksoud, M. Mailah, and A. M. Abdallah, "Robust intelligent self-tuning active force control of a quadrotor with improved body jerk performance," *IEEE Access*, vol. 8, pp. 150037–150050, 2020, doi: 10.1109/ACCESS.2020.3015101.

[23] K. Harshath, P. S. Manoharan, and M. Varatharajan, "Model predictive control of TRMS," in *Proc. Biennial Int. Conf. Power Energy Syst., Towards Sustain. Energy (PESTSE)*, Jan. 2016, pp. 1–5, doi: 10.1109/PESTSE.2016.7516455.

[24] S. Arimoto, S. Kawamura, and F. Miyazaki, "Convergence, stability and robustness of learning control schemes for robot manipulators," in *Proc. Int. Symp. Robot Manipulators Recent Trends Robot., Modeling, Control Edu.*, New York, NY, USA, 1986, pp. 307–316, Accessed: May 25, 2019. [Online]. Available: http://dl.acm.org/citation.cfm?id=23592.23632.

[25] J.-X. Xu and Y. Tan, *Linear and Nonlinear Iterative Learning Control*. Berlin, Germany: Springer-Verlag, 2003.

[26] R. Mascaró Palliser, R. Costa-Castelló, and G. A. Ramos, "Iterative learning control experimental results in twin-rotor device," *Math. Problems Eng.*, vol. 2017, Jan. 2017, Art. no. 6519497, doi: 10.1155/2017/6519497.

[27] M. Tahmasebi, M. Mailah, M. Gohari, and R. A. Rahman, "Vibration suppression of sprayer boom structure using active torque control and iterative learning. Part I: Modelling and control via simulation," *J. Vibrat. Control*, vol. 24, no. 20, pp. 4689–4699, Sep. 2017, doi: 10.1177/1077546317733164.

[28] *Quanser Inc*. Accessed: May 20, 2020. [Online]. Available: https://www.quanser.com

[29] *QUANSER AERO User Manual*, Quanser Inc., Ontario, ON, Canada, 2016.

**SHERIF I. ABDELMAKSOUD** received the M.S. degree in aerospace engineering from the King Fahd University of Petroleum and Minerals (KFUPM), Saudi Arabia, in 2015. He is currently pursuing the Ph.D. degree with the School of Mechanical Engineering, Universiti Teknologi Malaysia (UTM), Malaysia. His research interests include dynamic systems modeling, active force control, active vibration control, intelligent control systems, and autonomous unmanned aerial vehicles (UAVs).

**MUSA MAILAH** (Senior Member, IEEE) received the B.Eng. degree in mechanical engineering from Universiti Teknologi Malaysia (UTM), in 1988, and the M.Sc. degree in mechatronics and the Ph.D. degree in robot control and mechatronics from the University of Dundee, U.K., in 1992 and 1998, respectively. He is currently a Professor with the Faculty of Engineering, School of Mechanical Engineering, UTM, and the Head of the Intelligent Control and Automation (iCA) Research Group, UTM. His research interests include intelligent systems, active force control of dynamical systems, robot control, mobile manipulator, applied mechatronics, and industrial automation. He is also a registered Chartered Engineer (CEng), U.K.

**AYMAN M. ABDALLAH** received the B.S. and M.S. degrees in aerospace engineering from the King Fahd University of Petroleum and Minerals, Dhahran, Saudi Arabia, and the Ph.D. degree in aerospace engineering from Old Dominion University, Norfolk, VA, USA, in 2015. He is currently an Assistant Professor and the Chairman of the Aerospace Engineering Department, King Fahd University of Petroleum and Minerals. His research interests include new concept for aerodynamic attitude flight envelope, aircraft nonlinearity assessment, and flight dynamics and control.